Quantum Information Processing (2021) 20:233
https://doi.org/10.1007/s11128-021-03165-2

Implementation of efficient quantum search algorithms on NISQ computers

Kun Zhang[1] · Pooja Rao[2] · Kwangmin Yu[3] · Hyunkyung Lim[4] · Vladimir Korepin[5]

Received: 21 April 2021 / Accepted: 22 June 2021 / Published online: 10 July 2021

Abstract

Despite the advent of Grover's algorithm for the unstructured search, its successful implementation on near-term quantum devices is still limited. We apply three strategies to reduce the errors associated with implementing quantum search algorithms. Our improved search algorithms have been implemented on the IBM quantum processors. Using them, we demonstrate three- and four-qubit search algorithm with higher average success probabilities compared to previous works. We present the successful execution of the five-qubit search on the IBM quantum processor for the first time. The results have been benchmarked using degraded ratio, which is the ratio between the experimental and the theoretical success probabilities. The fast decay of the degraded ratio supports our divide-and-conquer strategy. Our proposed strategies are also useful for implementation of quantum search algorithms in the post-NISQ era.

✉ Kun Zhang
kun.h.zhang@stonybrook.edu

Pooja Rao
prao@msri.org

Kwangmin Yu
kyu@bnl.gov

Hyunkyung Lim
hyun-kyung.lim@stonybrook.edu

Vladimir Korepin
vladimir.korepin@stonybrook.edu

1 Department of Chemistry, State University of New York at Stony Brook, Stony Brook, NY 11794, USA

2 Mathematical Sciences Research Institute, Berkeley, CA 94720, USA

3 Computational Science Initiative, Brookhaven National Laboratory, Upton, NY 11973, USA

4 Department of Applied Mathematics and Statistics, Stony Brook University, Stony Brook, NY 11794, USA

5 C.N. Yang Institute for Theoretical Physics, Stony Brook university, Stony Brook, NY 11794-3840, USA

Keywords Quantum search algorithm · Depth optimization · Error mitigation · NISQ

1 Introduction

In recent years, much progress has been made in building quantum processors [1–4] and demonstrating quantum advantage [5,6]. In fact, quantum algorithms are the reason why quantum computers are so powerful [7]. However, the errors resulting from noisy quantum gates and decoherence make these devices far from perfect. The term “Noisy Intermediate-Scale Quantum” (NISQ) has been coined to describe the current era of noisy quantum computers [8].

Circuit depth is a practical metric for quantum circuits. Circuit depth is defined as the number of consecutive elementary operations required to run a circuit on quantum hardware. For the same circuit, different hardwares may give different depths since the connectivity may vary from machine to machine [9]. Most quantum computers have the elementary single- and two-qubit gates, but the running time of an algorithm on a quantum computer is directly related to the number of two-qubit gates. The two-qubit gates are much harder to realize in experiments (also take more time than single-qubit gates) since they create entanglement and the states become classically intractable [7]. Circuits with longer depths are more susceptible to gate and decoherence errors. Thus, NISQ era algorithms strive for shallow depths [10].

Grover’s algorithm is well-known for providing quadratic speedup for unstructured search problem [11,12]. It has wide applications, from exhaustive search for NP-hard problems [13] to quantum machine learning [14]. The theoretical complexity of Grover’s algorithm is based on number of queries to oracle, often referred to as the black box. The oracle can identify the target item in a database. Grover’s algorithm has been proven to be strictly optimal in the number of queries to the oracle [15,16].

Theoretical computational cost measures based on the oracular complexity, although useful for the theoretical analyses, are not very practical for assessing the performance of a quantum algorithm on real quantum machines. Given the wide-range of applications of Grover’s algorithm, a line of research has been directed towards estimating its implementation cost, including its depth and width requirements [17–20]. While querying the oracle is an important operation, it is not the sole operation in Grover’s algorithm. The other important part of Grover’s algorithm is the diffusion operator. Previous studies have shown that variants of Grover’s algorithm allow different choices for the diffusion operator, while maintaining the quantum speedup [21–23]. Partial diffusion operators, also called “local" diffusion operators, act on a subspace of the database. They are the key components in the partial search algorithms [24–26]. Interestingly, they can also be applied to the full search problem, decreasing the depth of the quantum search algorithms [27–30]. Such realizations make them much more viable for the NISQ devices.

Grover’s algorithm for up to four-qubit search domain ($2^4 = 16$ elements) has been implemented previously on the IBM quantum processors [31–33] for unstructured search. In this paper, we apply three different strategies to improve the performance of quantum search algorithms on the NISQ devices: (i) the hybrid classical-quantum search, (ii) use of partial diffusion operators to optimize the depth of quantum search

algorithms, and (iii) the divide-and-conquer search. Here the divide-and conquer means that we find the partial target string at each step. Since we are considering unstructured search problem, we do not recursively apply the divide-and-conquer strategy here. The three strategies can be jointly applied for an enhanced error mitigation. We demonstrate the improved three- and four-qubit search implementations over the standard Grover's algorithm. The success probabilities are higher than previous reported results [31,32]. For the five-qubit cases on IBM quantum processors, the search results from the direct execution of Grover's algorithms are too noisy, no better than the random guess. Our improved version, based on the proposed hybrid classical-quantum strategy, gives higher success probabilities than the purely classical approach (classical linear search). To the best of our knowledge, this is the first time that the five-qubit search algorithm has been successfully executed on IBM quantum processors. Note that the five-qubit search has recently been implemented on the trapped-ion qubits [34]. We benchmark our results using the degraded ratio of success probabilities. The fast decay of the degraded ratio observed in our results implies favoring of shallow depth circuits on IBM quantum processors.

This paper is organized as follows. In Sect. 2, we review full and partial search algorithms as well as introduce the notations used in our paper. In Sect. 3, we talk about three different strategies as mentioned above to improve the quantum search algorithms on real quantum devices. We present the results from executing these computational strategies on IBM's quantum computers in Sect. 4. Lastly, the conclusions from our study are presented in Sect. 5. Appendix includes more details on our notations and results presented in the main text.

2 Quantum search algorithms

First, we give a brief review of Grover's algorithm. Then we introduce the partial diffusion operator, a key component in our paper, that acts only on a subspace of the search domain.

2.1 Grover's algorithm

Grover's algorithm is realized by repeatedly applying the Grover operator, denoted as G_n, on the initial state $|s_n\rangle$ [11,12]. The symbol n denotes the number of qubits, which implies that the number of items in the database is $N = 2^n$. The initial state, $|s_n\rangle$, is uniform superposition of computational basis states of the Hilbert space, $\mathcal{H}_2^{\otimes n}$. It can be realized by applying the Hadamard gate, H, as [7]

$$|s_n\rangle = H^{\otimes n}|0\rangle^{\otimes n}. \tag{1}$$

Note that such a highly nontrivial initial state can easily be prepared with depth one.

The Grover operator, G_n, is a composition of two operators, the oracle and the diffusion operator. The oracle marks the target item and the diffusion operator creates an inversion about the mean. In Grover's algorithm, a query to the phase oracle results

in a sign flip on the target state. We denote the oracle operation as

$$O_t = \mathbb{1}_{2^n} - 2|t\rangle\langle t|. \tag{2}$$

Here, $|t\rangle$ is the target state representing the target string t. The target state $|t\rangle$ is also one of the computational basis states. We also refer to t as the target item or the target string in our paper. Operator $\mathbb{1}_{2^n}$ is the identity operator acting on $\mathcal{H}_2^{\otimes n}$. For convenience, we assume that there is a unique target state in the database. However, the depth reduction strategies in the next section do not limit to the case with a unique target state. The diffusion operator is independent of the oracle, and is defined as

$$D_n = 2|s_n\rangle\langle s_n| - \mathbb{1}_{2^n}. \tag{3}$$

The oracle operator, O_t, can be viewed as a reflection in the plane perpendicular to the target state $|t\rangle$. The diffusion operator, D_n, reflects the amplitude in the average, since the state, $|s_n\rangle$, is the equal superposition of all items in the database.

Composed of the oracle, O_t, and the diffusion operator, D_n, the Grover operator, G_n, is given by

$$G_n = D_n O_t. \tag{4}$$

Starting with the initial state, $|s_n\rangle$, and iteratively applying the Grover operator, G_n, on subsequent states, gives

$$P_n(j) = |\langle t|G_n^j|s_n\rangle|^2 = \sin^2((2j+1)\theta), \tag{5}$$

where $P_n(j)$ is the probability finding the target string t after j iterations of the Grover operator on the initial state. The angle θ is defined as $\sin\theta = 1/\sqrt{N}$. When j reaches $j_{\max} = \lfloor \pi\sqrt{N}/4 \rfloor$, the probability approaches unity. Thus, the oracular complexity of Grover's algorithm is $\mathcal{O}(\sqrt{N})$, which is quadratic speedup compared to the classical complexity, $\mathcal{O}(N)$. The idea behind Grover's algorithm is to increase the amplitude of the target state (approximately) linearly, which leads to a quadratic change in the probability as it is the amplitude squared. Moreover, Grover's algorithm is not limited to a specific initial state, such as the uniformly superimposed state, $|s_n\rangle$. As long as some distributions of the database can be efficiently realized, the amplitude of the target state can be amplified via Grover's algorithm. This general version of the algorithm is called the amplitude amplification algorithm [35,36].

Although the general formalism of Grover's algorithm is simple, realizing it on real quantum computers (for unstructured search problems) is a non-trivial question. Different search problems have different realizations of the oracle. Recent studies have shown how to construct the oracle (via the elementary quantum gates) for the AES key search [17,19,37,38] and the MAX-CUT problem [33]. The construction of diffusion operator on real quantum devices is more straightforward. The diffusion operator, D_n, and the n-qubit Toffoli gate denoted as $\Lambda_{n-1}(X)$, are single-qubit-gate equivalent [7]. The notation X denotes the NOT gate, while $n-1$ means that there are $n-1$ control qubits. For example, when $n = 2$, $\Lambda_{n-1}(X)$ gives the CNOT gate. The n-qubit Toffoli

gate $\Lambda_{n-1}(X)$ can be decomposed as a combination of single- and two-qubit gates with the depth linear in n (with ancillary qubits) [39].

2.2 Partial diffusion operator

The diffusion operator, D_n, defined in Eq. (3), reflects the amplitudes in the average of all items. We can generalize such an operator as

$$D_{n,m} = \mathbb{1}_{2^{n-m}} \otimes (2|s_m\rangle\langle s_m| - \mathbb{1}_{2^m}), \tag{6}$$

with $m \leq n$. The diffusion operator, $D_{n,m}$, only reflects the amplitude in the subspace of the database. As $m < n$, we refer to $D_{n,m}$ as the local or partial diffusion operator. For convenience, we drop n from the notation to denote $D_m \equiv D_{n,m}$, without any possibility of confusion. Combined with the oracle operator, O_t, the local Grover operator is defined as

$$G_m = D_m O_t. \tag{7}$$

Note that G_m is still an n-qubit operator since the oracle acts on the full n-qubit space.

The local diffusion operator can naturally solve the partial search problem [24–26], which finds the substring of the target state. For example, the target state $|t\rangle$, can be decomposed as $|t\rangle = |t_1\rangle \otimes |t_2\rangle$. Assume that t_1 is $(n-m)$-bit length while t_2 is m-bit length. We can think that the database is divided into $K = 2^{n-m}$ blocks. Each block has $b = 2^m$ number of items ($N = bK$). Also, each block has the partial target string t_2. The quantum partial search algorithm (QPSA) finds the target block represented by the target string t_1. The target string t_2 is not concerned.

The most efficient QPSA (based on the oracular complexity) starts by running the global Grover operators first, followed by running the local Grover operators and lastly, runs a single global Grover operator [40]. Note that the operators, G_n and G_m, do not commute [41]. Thus, different orders of operators give different success probabilities. The QPSA trades accuracy for speed (based on the oracular complexity). The QPSA finds the target substring t_1, with fewer queries to the oracle than the full search algorithm. The reduced number of oracles, compared to Grover's algorithm, scales as $\sqrt{b}$ [24–26].

Although QPSA is the main application of the local diffusion operator, Grover introduced the local diffusion operator before the invention of QPSA. The local diffusion operator, introduced in [27], aims to reduce the total number of gates in the quantum search algorithm. This motivation is easy to see as the partial diffusion operator, D_m, can be realized with fewer elementary quantum gates than the global diffusion operator, D_n, with $n > m$. Recent studies have revealed several other ways to reduce the depth of quantum search algorithm by exploiting the partial diffusion operator [28,29]. We will discuss different strategies to improve the performance of quantum search algorithms on real devices in the next section.

3 Strategies to improve quantum search algorithms

In this section, we present three different strategies to improve accuracy and efficiency of the quantum search algorithm on the NISQ processors. Every strategy utilizes the local diffusion operator, D_m, as defined in Eq. (6). In NISQ era, such strategies are important because they reduce the depth of the circuits. In post-NISQ era, such strategies can potentially reduce the physical resources needed for error correction, as well as the running time of the algorithms.

3.1 Hybrid search algorithm

The local diffusion operator, D_m, only acts on the subset of the given database. We can renormalize the search space in order to exploit D_m. Suppose that the search problem is to find the target string t with length n. The oracle can only recognize the target state $|t\rangle$. By renormalizing the search space, we prepare the initial state $|t_1'\rangle \otimes |s_m\rangle$, where t_1' is a specific string with length $(n-m)$. If $t_1' = t_1$ ($|t\rangle = |t_1\rangle \otimes |t_2\rangle$), then using Eq. (5), the probability of finding t_2 after j iterations of G_m on $|t_1\rangle \otimes |s_m\rangle$ is

$$P_m(j) = \sin^2((2j+1)\theta_b), \tag{8}$$

with $\sin\theta_b = 1/\sqrt{b}$ and $b = 2^m$.

Let the probability that t_1' is t_1 be $P(t_1' = t_1)$. The probability $P_m(j)$ is conditioned on the probability $P(t_1' = t_1)$. Then the total probability of finding the target string t with j iterations of G_m is

$$P_n'(j) = P(t_1' = t_1)P_m(j). \tag{9}$$

For the unstructured search problem, the classical probability, $P(t_1' = t_1)$, can only be given by randomly guessing on 2^{n-m} bits, i.e., $P(t_1' = t_1) = 1/2^{n-m}$. Random guessing does not require any quantum computational resources. We call such a search method as the hybrid classical-quantum search algorithm.

The advantage for the hybrid classical-quantum search algorithm is twofold. First, the depth of G_m is smaller than G_n. If the total depth is fixed, the hybrid classical-quantum algorithm can apply more iterations of oracle. Second, quantum coherence during the algorithm is only required on the subspace $\mathcal{H}_2^{\otimes m}$. The full search algorithm is based on the coherence on $\mathcal{H}_2^{\otimes n}$, which is more fragile. Although the theoretical success probability is always smaller than the full search success probability with the same number of oracles, the real success probability could be higher because of its shorter depth and limited coherence between qubits. The theoretical success probability of hybrid search decays exponentially with respect to the number of randomly guessed qubits. Therefore, we do not expect a large number of randomly guessed qubits, especially for a large database. Therefore, the hybrid strategy may not be suitable for post-NISQ search problems.

3.2 Depth optimization by partial diffusion operators

Grover's algorithm is optimal in the number of queries to the oracle [15,16]. However, the oracular complexity is not the only metric for determining an algorithm's requirement of the physical computational resources (such as the depth and the width of the circuit). The Grover operator is a combination of oracle operator and diffusion operator. The depth of the quantum search circuit can be reduced if we replace the global diffusion operator D_n by the local diffusion operator D_m. There are different ways to do such replacements [27–30]. Here, we follow the ideas from [29], which provides a general framework for depth optimization.

Suppose that we design the search circuits by the operator

$$S_{n,m}(\tilde{j}) = G_n^{j_1} G_m^{j_2} \cdots G_n^{j_{q-1}} G_m^{j_q}, \tag{10}$$

with $\tilde{j} = \{j_1, j_2, \ldots, j_q\}$. Every local diffusion operator acts on the same subspace. To remove the ambiguity of the notation $S_{n,m}(\tilde{j})$, we require that the last number j_q is always for the local Grover operator. For example, $S_{6,4}(\{2, 0\}) = G_6^2$ and $S_{6,4}(\{1, 1\}) = G_6 G_4$. Note that $S_{n,m}(\{j, 0\}) = G_n^j$ is the standard Grover's algorithm. We only consider one kind of local diffusion operator here. The idea below can be generalized to multi-type local diffusion operators local diffusion operators acting on different sizes of blocks, which gives the search operator $S_{n,m_1,m_2,\cdots,m_k}$.

The success probability of finding the target state by the operator $S_{n,m}(\tilde{j})$ is

$$P_{n,m}(\tilde{j}) = |\langle t|S_{n,m}(\tilde{j})|s_n\rangle|^2. \tag{11}$$

Since Grover's algorithm is strictly optimal in number of queries to the oracle [16], a local diffusion operator can only decrease the success probability compared to Grover's algorithm (with the fixed number of oracles). For example, $P_{n,m}(\{j_1, j_2\}) \leq P_{n,m}(\{j_1 + j_2, 0\})$.

The physical resources of quantum computers are the depth and the width. The depth roughly represents the physical running time of the circuit. We denote the depth of operator U as $d(U)$. For the same operator, different devices may have different depths due to the different connectivity of the qubits and the different sets of universal gates. Operator $S_{n,m}(\tilde{j})$ can have lower depth compared to G_n^j (with the same number of oracles). For example, $d(S_{n,m}(\{j_1, j_2\})) \leq d(S_{n,m}(\{j_1 + j_2, 0\}))$. We introduce the expected depth of the search circuit $S_{n,m}(\tilde{j}))$ as

$$\langle d_{n,m}(\tilde{j})\rangle = \frac{d(S_{n,m}(\tilde{j}))}{P_{n,m}(\tilde{j})}. \tag{12}$$

Then the depth optimization strategy is to find the minimum of $\langle d_{n,m}(\tilde{j})\rangle$ given by

$$\langle d_n\rangle = \min_{m,\tilde{j}} \langle d_{n,m}(\tilde{j})\rangle. \tag{13}$$

We also optimize the size of the local diffusion operator given by the parameter m. Although we apply the local diffusion operator in $S_{n,m}(\tilde{j})$, our algorithm is not the partial search algorithm.

The minimal expected number of oracles for Grover's algorithm is studied in [15,42]. Recall that the maximal iteration (giving the maximal success probability) is $j_{\max} = \lfloor \pi\sqrt{N}/4 \rfloor$. However, the minimal expected number of oracles is given by $j_{\exp} = \lfloor 0.583\sqrt{N} \rfloor$, which is smaller than $j_{\max}$. Incorporating the depth of global Grover operator $d(G_n)$, the optimal iteration number, $j_{\exp}$, can give the minimal expected depth of Grover's algorithm. The significance of $\langle d_n \rangle$ (given by the partial diffusion operator) is to win over the minimal expected depth of Grover's algorithm. Theoretical study shows that there is a critical depth ratio (the ratio between the depths of the oracle and the global diffusion operator), below which Grover's algorithm is not optimal in depth [29]. Such a critical depth ratio scales as $\mathcal{O}(n^{-1}2^{n/2})$. For example in the 10-qubit search, the second strategy can be applied if the depth of oracle is smaller than 83.97 times the depth of the 10-qubit Toffoli gate. In practice, we would not have such a large oracle depth. For example, based on the data in [19], the depth of AES-128 oracle is around 10 times the depth of global diffusion operator.

3.3 Divide-and-conquer strategy

NISQ devices can only run shallow depth circuits [8]. Recent benchmarking results suggest that the fidelity of a circuit does not linearly decrease with the depth of two-qubit gates [32]. If we can reinitialize the input during the algorithm, then we can prevent the accumulation of errors at subsequent stages. The divide-and-conquer search algorithm is naturally related to QPSA. We can find partial bits of the target item, then renormalize the database to find the rest of the target string.

For simplicity, we consider the two-stage quantum search algorithm. It can be easily generalized into the multi-stage search algorithm. In the first stage, the task is to find the target substring, t_1, with high probability. The second stage finds the rest target string, t_2. The second-stage circuit will be dependent on the results from the first stage. The underlying idea behind the two-stage search algorithm is similar to the idea behind the hybrid classical-quantum search algorithm in Sect. 3.1. The difference is that both the stages are realized by quantum search algorithms. Suppose that the first stage is realized by the operator $S^{(1)}_{n,m}(\tilde{j})$. The initial state for the first stage is $|s_n\rangle$. The probability finding the target substring, t_1, is given by

$$P^{(1)}_{n,m}(\tilde{j}) = \mathrm{Tr}\left[(|t_1\rangle\langle t_1| \otimes \mathbb{1}_{2^m})\, S^{(1)}_{n,m}(\tilde{j}) |s_n\rangle\langle s_n| S^{(1)}_{n,m}(\tilde{j})^\dagger \right]. \tag{14}$$

The diffusion operator, D_m, in $S^{(1)}_{n,m}(\tilde{j})$ acts on the qubits within the target substring, t_2. In other words, we measure the qubits which are not acted upon by D_m. Such a circuit design comes from QPSA.

Suppose we find t_1 at the first stage. We prepare the initial state $|t_1\rangle \otimes |s_m\rangle$. Then design the operator $S^{(2)}_{n,m'}$ with $m' < m$ for the second stage. Such a circuit is the normalized version of the full search algorithm. The probability of finding the remaining

target string t_2 is

$$P^{(2)}_{n,m}(\tilde{j}') = \mathrm{Tr}\left[(\mathbb{1}_{2^{n-m}} \otimes |t_2\rangle\langle t_2|)\, S^{(2)}_{n,m'}(\tilde{j}')|t_1, s_m\rangle\langle t_1, s_m| S^{(2)}_{n,m'}(\tilde{j}')^\dagger \right], \tag{15}$$

with short notation $|t_1, s_m\rangle = |t_1\rangle \otimes |s_m\rangle$. The operator $S^{(2)}_{n,m'}$ does not change the initial state $|t_1\rangle$.

The expected depth of the above two-stage search algorithm is

$$\langle d_{n,m,m'}(\tilde{j}, \tilde{j}')\rangle = \frac{d(S^{(1)}_{n,m}(\tilde{j})) + d(S^{(2)}_{n,m'}(\tilde{j}'))}{P^{(1)}_{n,m}(\tilde{j})\, P^{(2)}_{n,m}(\tilde{j}')}. \tag{16}$$

The minimal expected depth can be obtained by optimizing the operators and the size of the diffusion operators:

$$\langle d_{n,2}\rangle = \min_{m,m',\tilde{j},\tilde{j}'} \langle d_{n,m,m'}(\tilde{j}, \tilde{j}')\rangle \tag{17}$$

We add a subscript 2 in $\langle d_{n,2}\rangle$ to distinguish the minimal expected depth of the full search $\langle d_n\rangle$ in Eq. (13). It is expected that $\langle d_{n,2}\rangle < \langle d_n\rangle$, since the measurement in the middle wipes out the amplified amplitude of the state $|t_2\rangle$. Only when the depth of the oracle is comparable to the depth of the global diffusion operator, the two-stage search algorithm can have lower depth than Grover's algorithm [29].

The motivation for the multi-stage circuits is to mitigate the errors. Another advantage of the multi-stage search circuit is its ability to run the quantum search algorithm in parallel [29,42]. We can assign the first stage circuit to different quantum computers. Then each device finds a different part of the target string t. Combining all the results gives the full target string.

4 Implementation on IBM quantum processors

First, we briefly present the basic setup as well as the circuit design from our implementation of the algorithms on the IBM quantum processors. Then we discuss the results on the three-, four-, and five-qubit search in the following subsections.

4.1 Circuit designs

The target item t is encoded in the oracle. We have assumed the uniqueness of the target item. As toy model, we choose the phase oracle presented in [3]. The n-qubit phase oracle is single-qubit-gate-equivalent to the n-qubit Toffoli gate $\Lambda_{n-1}(X)$ (or the n-qubit controlled phase gate $\Lambda_{n-1}(Z)$). Note that the diffusion operator D_n is also single-qubit-gate-equivalent to the n-qubit Toffoli gate $\Lambda_{n-1}(X)$ [7]. Although Qiskit provides the built-in n-qubit controlled gate, its fidelity and efficiency are not optimal. In the following, we show the realizations of three-, four-, and five-qubit controlled phase gate $\Lambda_{n-1}(Z)$ from our implementation.

It is well-known that the three-qubit controlled phase gate, $\Lambda_2(Z)$ (or the Toffoli gate $\Lambda_2(X)$), can be realized by six CNOT gates, with full connectivity between the three qubits [7]. Qubits with linear connectivity need additional SWAP gates for such a realization. In [32], Gwinner et al. provide a way to realize the three-qubit controlled phase gate $\Lambda_2(Z)$ via eight CNOT gates on linearly connected qubits, shown below.

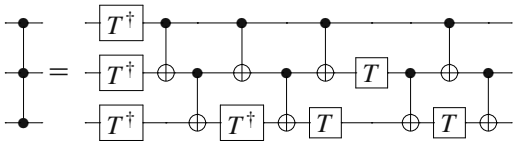

(18)

Here, T is $\pi/8$ gate given by $T = \mathrm{diag}\{1, e^{i\pi/4}\}$ with $i = \sqrt{-1}$.

The four-qubit gate $\Lambda_3(Z)$ can be realized by three $\Lambda_2(Z)$ gates in a V-shape design (with one clean ancillary qubit) [39]. As pointed in [43], we can take advantages of the relative-phase Toffoli gate to reduce the resources of n-qubit Toffoli gate constructions. The three-qubit controlled Y gate ($Y = ZX$) can be realized as [44]

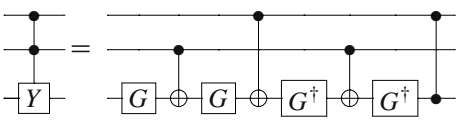

(19)

with the y-axis rotation gate $G = R_y(\pi/4)$. Then the four-qubit controlled phase gate $\Lambda_3(Z)$ can be constructed as

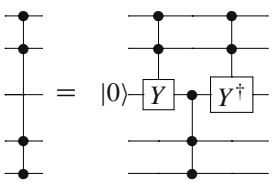

(20)

with one ancillary qubit $|0\rangle$. The rightmost CZ gate in circuit (19) can be cancelled with the CZ gate in $\Lambda_2(Y^\dagger)$ when the above $\Lambda_3(Z)$ gate is realized. Note that the CZ gate commutes with the $\Lambda_2(Z)$ gate.

Similar to the realization of $\Lambda_3(Z)$ gate, we design the five-qubit controlled phase gate $\Lambda_4(Z)$ via two four-qubit controlled-Y gates $\Lambda_3(Y)$ and one three-qubit controlled phase gate $\Lambda_2(Z)$, in addition to one clean ancillary qubit. The four-qubit controlled gates $\Lambda_3(Y)$ can be decomposed as [43]

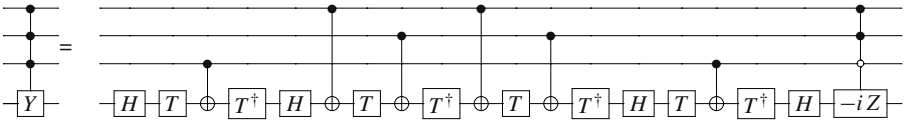

(21)

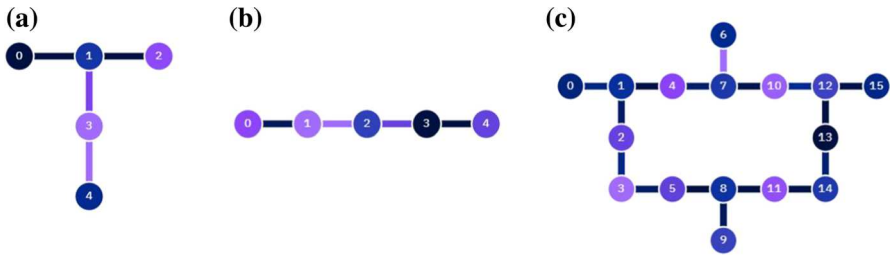

Fig. 1 Qubits layout of the IBM quantum processors. **a** The five-qubit system, named as Vigo, has the "T" connectivity. **b** The five-qubit system, named as Athens, has the linear connectivity. **c** The sixteen-qubit system, is named as Guadalupe. The color on dots represent for the frequency of each qubit. The color on connectivities represent for the error rate of two-qubit gate on the connected two qubits (Color figure online)

Above circuit requires that the target qubit connects all the control qubits. The rightmost four-qubit controlled gate gives a relative phase $\mp i$ to the states $|1100\rangle$ and $|1101\rangle$, respectively. We do not need to physically realize such gate since it would be cancelled with its inverse in the realization of the $\Lambda_4(Z)$ gate, as shown below.

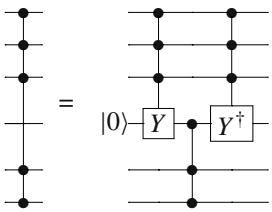

(22)

We can also design the $\Lambda_4(Z)$ gate via four $\Lambda_2(Y)$ gates and one $\Lambda_2(Z)$ gate, which requires two clean ancillary qubits. Although this realization has fewer CNOT gates, its fidelity is lower. Seven-qubit superposition is more fragile than the superposition on the six qubits.

4.2 Setup

We run each circuit with randomly chosen target states in 30 trials. In each trial, the circuit is run with 8192 shots to calculate the success probability. We use the same 30 random target states for different search circuits, in order to compare the results between different search circuits. Since in the unstructured search problem, any target state is equally possible. Random chosen target state is more closed to the practical situation. Besides, state $|1\rangle$ relaxes to the ground state $|0\rangle$ with some probability. Therefore, target strings with larger Hamming weights have lower success probabilities on real devices. Random chosen target state can also mitigate such biases. To make sure that the random chosen target states are not biased, we list those target states in "Appendix A".

IBM provides processors with different number of qubits, ranging from one qubit to sixty five qubits. For our purposes, we implement the three-qubit search circuits

on the five-qubit processor, Vigo. The four-qubit search circuits are implemented on both Vigo (the five-qubit backend with "T" connectivity) and Athens (the five-qubit backend with linear connectivity). The five-qubit search circuits are tested on the sixteen-qubit system, Guadalupe. See Fig. 1 for the topological layout of the qubits in different processors. Note that the connectivity of Vigo is better than the connectivity of Athens. However, Athens has lower gate error rates in average than Vigo. In terms of the metric quantum volume, which characterizes the largest random circuit of equal width and depth that the computer successfully implements [9], Athens has quantum volume 32 while Vigo has 16.

Besides the success probability of the circuit, we also record the depth of each circuit. The depth is obtained after compiling for each specified backend. The depth obtained in this way represents the real operational length of the circuit. Every quantum processor can only perform four different gates (called the universal gate set) - z-axis rotation gate, X gate, square root X gate and CNOT gate. Oracles encoded different target states have slightly different depths. Combining the success probability and the circuit depth, we calculate the expected depth according to Eqs. (12) and (16), for the single- and two-stage circuits, respectively.

Recently, Wang et al. introduced the selectivity parameter, S, to quantify how distinct the signal is compared to the next most probable outcome [20]. The selectivity is also separately proposed in [45], called inference strength. It is important for understanding the quality of results obtained by a search algorithm on real devices. For our purposes, we simply treat it as the ratio between P_t (the probability of obtaining the target string) and the maximum of P_{nt} (the probability of obtaining the non-target string), defined by

$$S = \frac{P_t}{\max\{P_{nt}\}}. \tag{23}$$

Selectivity less than 1 suggests the failure of the implementation. Note that the amplitudes of non-target states are never amplified in the quantum search algorithms. For the classical-quantum hybrid circuit, we only consider the selectivity for the results obtained from the quantum algorithm. In other words, P_t is the probability of obtaining the target substring. For the multi-stage circuits, we choose the minimal selectivity among the circuits from the different stages. Note that the selectivity reveals the probabilistic distribution of the implementation results, rather than a theoretical parameter.

We also benchmark the results via the degraded ratio, defined as

$$R_{\text{IBMq}} = \frac{P_{\text{IBMq}}}{P_{\text{theo}}}. \tag{24}$$

Here, the probability P_{theo} is the theoretical success probability of finding the target string (the theoretical success probability of the search circuit); probability P_{IBMq} is the success probability obtained from the IBM quantum processors. Degraded ratio has been reported to decay exponentially with the number of two-qubit gates in [32]. Such fast degradation is the motivation for our multi-stage strategy.

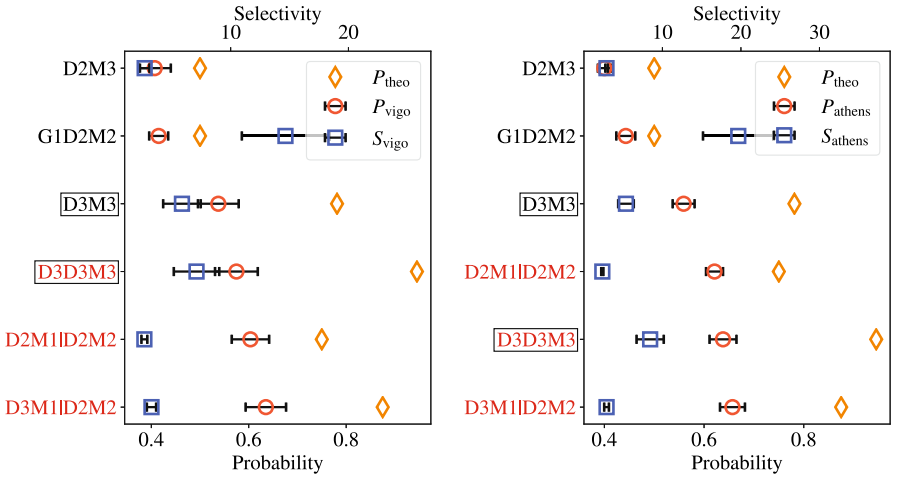

Fig. 2 Success probabilities of the three-qubit search circuits on the IBM quantum processors Vigo (left) and Athens (right). Circuit names with black and red colors are the circuits with one and two oracles, respectively. The standard Grover's algorithm circuits are boxed. Circuits are ordered as the magnitude of the success probabilities obtained from the Vigo machine (red circle). Standard deviations are obtained from 30 trials with random target states. Each trial has 8192 shots (Color figure online)

For different circuits, we use the following notations. The Grover operator with the diffusion operator D_m is denoted as Dm. Measurement on p qubits is Mp. If there is a classical initialization on q number of qubits, then it is Gq (see the hybrid search algorithm in Sect. 3.1). Note that the italic notation G_m is for the Grover operator defined in Eq. (7). The left to right ordering represents the order in which these operations are carried out. We always specify the search domain for each circuit notations. For example, the three-qubit search circuit G1D2M2 represents the random initialization of one qubit followed by the Grover operator with a two-qubit diffusion operator and then measure these two qubits.

For the two-stage algorithm, we follow the same rules, but each of the stages is separated by a vertical line "|". For example, the three-qubit search circuit D2M1|D2M2 is a two-stage algorithm. In the first stage, the Grover operator G_2 (with two-qubit diffusion operator) is applied, then one of the qubits is measured (acted upon by the diffusion operator). The second stage is to initialize the state according to the results from the first stage (see Sect. 3.3 for details), then apply the Grover operator G_2 (with two-qubit diffusion operator) followed by the measurement on the two qubits (to be searched). A list of explanations on all the circuit notations can be found in Appendix. See Table 4 for the three-qubit search circuits and Table 7 for the four-qubit search circuits.

4.3 Three-qubit cases

Three-qubit Grover's algorithm gives the theoretical success probabilities of 0.781 and 0.945 with one and two Grover iterations, respectively. These two circuits are

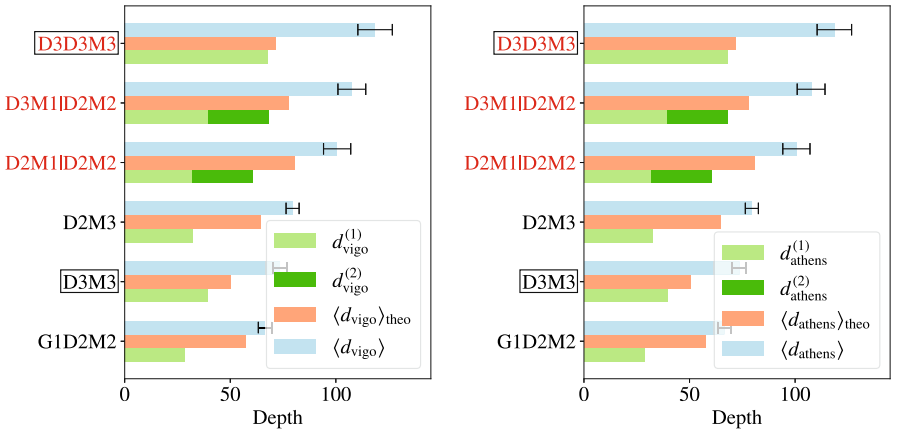

Fig. 3 Circuit depths and expected depths of the three-qubit search circuits on the IBM quantum processors Vigo (left) and Athens (right). Here $d^{(1)}$ or $d^{(2)}$ is the depth of first or second stage circuit; $\langle d_{\text{vigo}}\rangle_{\text{theo}}$ or $\langle d_{\text{athens}}\rangle_{\text{theo}}$ is the theoretical expected depth of the circuit (given by the theoretical success probability) on Vigo or Athens; $\langle d_{\text{vigo}}\rangle$ or $\langle d_{\text{athens}}\rangle$is the real expected depth of the circuit (given by the real success probability) on Vigo or Athens. Circuit names with black and red colors indicate the circuits with one and two oracles, respectively. The standard Grover's algorithm circuits are boxed. Circuits are ordered according to the magnitude of the expected depth obtained from the Vigo machine (top blue bar). Standard deviations are obtained from 30 trials with random target states. Each trial has 8192 shots (Color figure online)

denoted as D3M3 and D3D3M3. We design another two circuits with one oracle, i.e., D2M3 and G1D2M2, which both give the 0.5 theoretical success probabilities. We design two different two-stage three-qubit search circuits. They both find one bit of the target in the first stage. One uses the three-qubit diffusion operator, i.e., D3M1, the other uses the two-qubit diffusion operator, i.e., D2M1. In the second stage, the circuits are equivalent to the two-qubit search, which gives success probability as 1 with just a single Grover iteration, i.e., D2M2. The detailed explanations about these six circuits can be found in Appendix (Table 4).

We plot the success probabilities, as well as the selectivities, of the three-qubit search circuits in Fig. 2. The detailed data, as well as the thirty random target states, can be found in "Appendix A". To exclude any possible biases from the random target states, we also provide supplementary data based on the average target states in "Appendix B' (Table 11). Both on the Vigo and Athens machines, the two-stage circuit D3M1|D2M2 gives the largest success probabilities. Both the two-stage circuits have higher success probabilities than Grover's realization D3D3M3, though D3D3M3 has the largest theoretical success probability. Such results demonstrate the significance of the divide-and-conquer strategy. The circuit G1D2M2 has the largest selectivity, which shows its robustness against the errors. The circuits D2M3 and G1D2M2 have the identical implementations except for the initial states. The success probability of G1D2M2 is slightly higher than D2M3 because the latter is only manipulating the two-qubit superposition states.

Incorporating the circuit depth with their success probabilities, we plot the expected depth in Fig. 3. There are three different categories of the depth parameter. The first is the depth of the circuit, such as d(D3M3). The second is the theoretical expected depth,

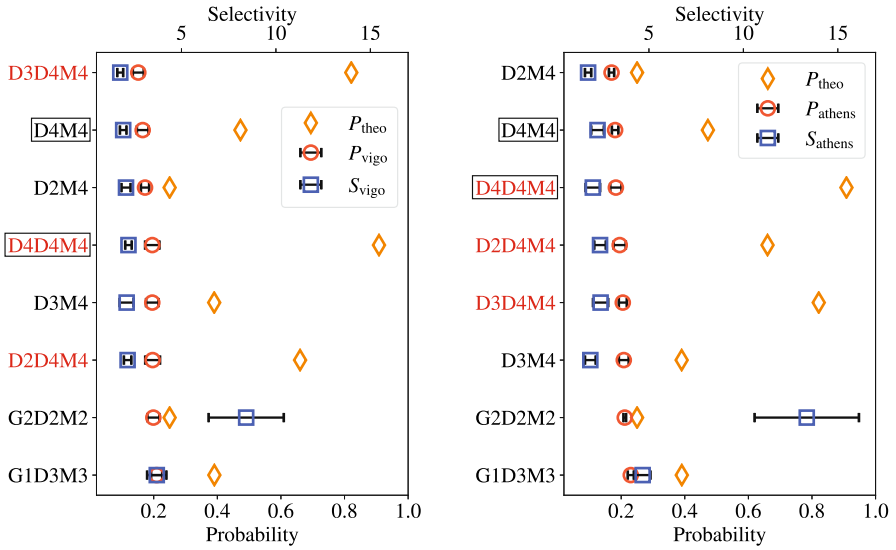

Fig. 4 Probabilities of the one-stage four-qubit search circuits on the IBM quantum processor Vigo (left figure) and Athens (right figure). Circuit names with black and red color are circuits with one and two oracles, respectively. The standard Grover's algorithm circuits are boxed. Circuits are ordered according to the magnitude of the success probabilities (red circle). Standard deviations are obtained from 30 trials with random target states. Each trial has 8192 shots (Color figure online)

given by the theoretical success probability of the circuits. The last is the expected depth on real machines, given by the success probabilities obtained from the IBM quantum processors. The least expected depth on the Vigo and Athens machines are both given by the circuit G1D2M2. Although G1D2M2 has lower success probability than D3M3, its shallow depth can find the target state more efficiently. The two two-stage circuits have lower expected depth than Grover's D3D3M3, since they have lower depth realizations while maintaining higher success probabilities. Both D3M3 and D3D3M3 are the standard Grover's algorithm. Neither the one-oracle D3M3 nor the two-oracle D3D3M3 gives the optimal expected depth. Depth optimizations for the search algorithm are necessary when running on the real quantum devices.

4.4 Four-qubit cases

Four-qubit search has more scope for exploiting the partial diffusion operators than the three-qubit search. Including the standard Grover's algorithm with one and two oracles, we design a total of fourteen different circuits and test them on both the Vigo and Athens processors. See Appendix (Table 7) for detailed explanations on each circuit. Among the fourteen circuits, eight are one-stage circuits and six are two-stage circuits. Success probabilities of the one-stage circuits are plotted in Fig. 4. For the two-stage circuits, the success probabilities are plotted in Fig. 5. Also see Table 3 in "Appendix A" for the thirty random target states. The supplementary data on the average target states can be found in "Appendix B" (Table 12).

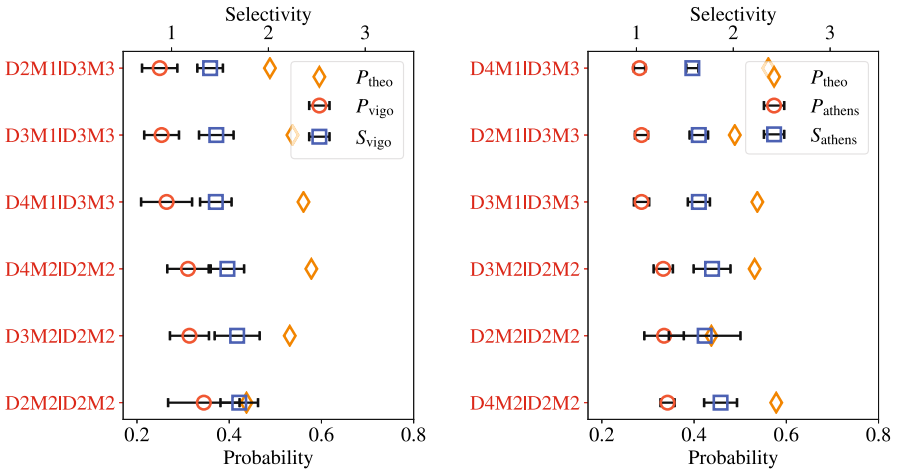

Fig. 5 Probabilities of the two-stage four-qubit search circuits on the IBM quantum processor Vigo (left figure) and Athens (right figure). Circuits are ordered according to the magnitude of the success probabilities (red circle). Standard deviations are obtained from 30 trials with random target states. Each trial has 8192 shots (Color figure online)

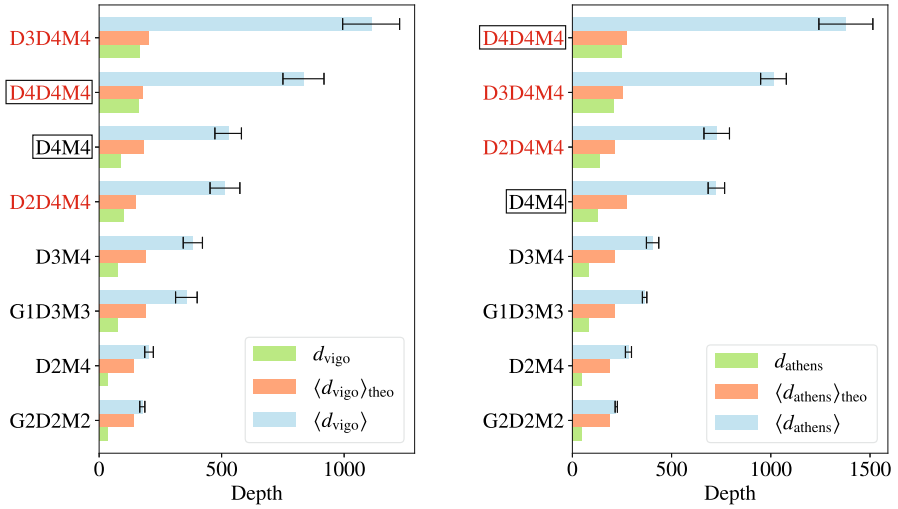

Fig. 6 Circuit depths and expected depths of the one-stage four-qubit search circuits on the IBM quantum processor Vigo (left figure) and Athens (right figure). Here d_{vigo} or d_{athens} is the circuit depth on Vigo or Athens; $\langle d_{\text{vigo}}\rangle_{\text{theo}}$ or $\langle d_{\text{athens}}\rangle_{\text{theo}}$ is the theoretical expected depth of the circuit (given by the theoretical success probability) on Vigo or Athens; $\langle d_{\text{vigo}}\rangle$ or $\langle d_{\text{athens}}\rangle$is the real expected depth of the circuit (given by the real success probability) on Vigo or Athens. Circuit names with black and red colors are circuits with one and two oracles, respectively. The standard Grover's algorithm circuits are boxed. Circuits are ordered according to the magnitude of the expected depth (top blue bar). Standard deviations are obtained from 30 trials with random target states. Each trial has 8192 shots (Color figure online)

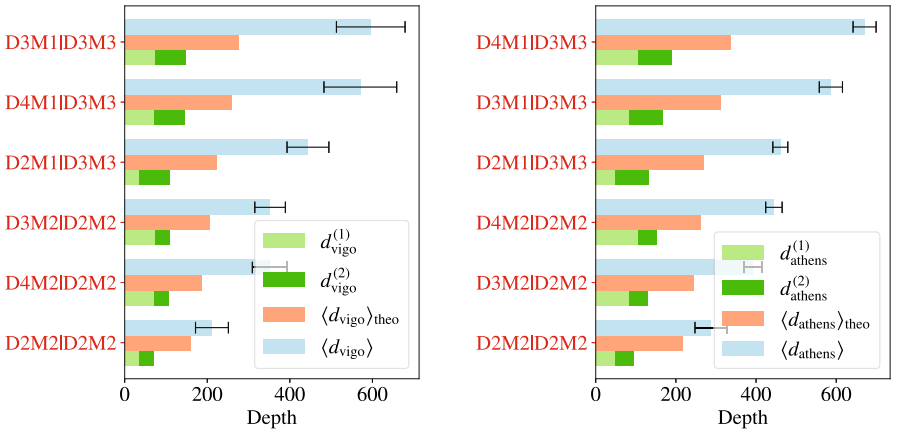

Fig. 7 Circuit depths and expected depths of the two-stage four-qubit search circuits on the IBM quantum processor Vigo (left figure) and Athens (right figure). Here $d^{(1)}$ or $d^{(2)}$ is the depth of first or second stage circuit; $\langle d_{\text{vigo}}\rangle_{\text{theo}}$ or $\langle d_{\text{athens}}\rangle_{\text{theo}}$ is the theoretical expected depth of the circuit (given by the theoretical success probability) on Vigo or Athens; $\langle d_{\text{vigo}}\rangle$ or $\langle d_{\text{athens}}\rangle$is the real expected depth of the circuit (given by the real success probability) on Vigo or Athens. Circuits are ordered according to the magnitude of the expected depth (top blue bar). Standard deviations are obtained from 30 trials with random target states. Each trial has 8192 shots (Color figure online)

Among the eight one-stage search circuits, D4D4M4 gives the largest theoretical probability 0.908. However, the real success probability is degraded below to 0.2 (both on Vigo and Athens) due to the actual implementation that has longer depth. On Vigo and Athens both, G1D3M3 gives the largest success probability among the one-stage circuits on real machines. On the Vigo machine, the two-oracle circuit D2D4M4 has larger success probability than the Grover's two-oracle circuit D4D4M4. Similar results are found on Athens. Local diffusion operators may decrease the theoretical success probability, but its low depth overcomes such disadvantages on quantum devices.

For more information on the two-stage circuits, see Fig. 5. There are two types of two-stage four-qubit circuits. One type finds a target bit at the first stage; then finds the rest of the three target bits in the second stage. The other type searches two target bits in each of the two stages, which provides a higher probability than the first dividing strategy. Circuits implemented on Vigo have quite similar results on Athens. The two-stage circuit, D2M2|D2M2, gives the average success probability of 0.345. The two-oracle Grover's search, D4D4M4, has the average success probability of 0.195. Notably, our divide-and-conquer circuit D2M2|D2M2 nearly doubles the success probability of the standard Grover's circuit D4D4M4. Compared to a recent study [32], our success probability for the four-qubit search algorithm exceeds 0.3, which is significant.

For the depth (the circuit depth, the theoretical expected depth and the expected depth on the real devices) of the one-stage and the two-stage four-qubit search circuits, see Figs. 6 and 7 . Note that because of the better connectivity of the Vigo, every circuit has slightly longer depth on Athens as compared to Vigo. The averaged circuit depth

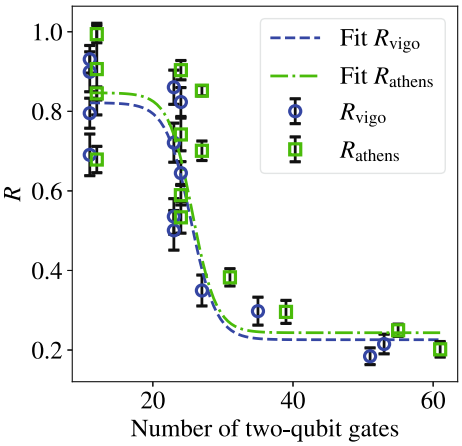

Fig. 8 Degraded ratio of the success probabilities vs. the number of two-qubit gates. The curve is fitted according to the logistic function. If the number of two-qubit gates exceeds thirty, the noise may lead to an inefficient search (Color figure online)

of G2D2M2 is less than the half of one-oracle Grover's circuit D4M4. However, the overall success probability of G2D2M2 is higher than D4M4. The expected depth of circuit G2D2M2 is far shorter than that of D4M4. The circuit G2D2M2 has the shortest theoretical expected depth both on the Vigo and Athens.

In the two-stage circuits, the two-two dividing has shorter depth than the one-three dividing. The two-two dividing exploits the local diffusion operator more efficiently. Note that the one-qubit quantum search algorithm is not well defined; therefore we do not have the three-one dividing. The expected depth of two-oracle Grover's circuit D4D4M4 is > 800 (833.99 on Vigo and 1378.31 on Athens). The divide-and-conquer circuit (D2M2|D2M2) suppresses the expected depth below 300 (211.35 on Vigo and 287.58 on Athens).

Quantum algorithms with long circuits cannot be directly divided into several stages, with new initialized states during the algorithm. Measurements in the middle will wipe out the established coherence between qubits. Suppose that the long circuit has the success probability of p. Dividing it into two parts gives the success probabilities p_1 and p_2 for each part, respectively. Previous theoretical study shows that $p > p_1 p_2$ [29]. However, our tests demonstrate that $p' < p'_1 p'_2$ on real quantum computers. The explanation relies on benchmarking the parameter, the degraded ratio R, defined in Eq. (24). Based on our data from the four-qubit search circuits, we plot the degraded ratio versus the number of two-qubit gates in Fig. 8. The degraded ratio drops dramatically when the circuits have more than 30 two-qubit gates. In other words, if the number of two-qubit gates exceeds thirty, the noises may surpass the amplified amplitude of the target state. The data is fitted by the logistic function

$$R(x) = \frac{a}{1 + \exp(-b(x - c))} + d. \tag{25}$$

Here, x is the number of two-qubit gates and the numbers $\{a, b, c, d\}$ are the parameters to be fitted. Similar benchmarking results have been reported in [32]. This exponential drop is the motivation for our divide-and-conquer designs and explains why the divide-and-conquer circuits have better performance than the one-stage circuits.

4.5 Five-qubit cases

To the best of our knowledge, the five-qubit search algorithm has never been successfully implemented on any of the IBM quantum processors. The five-qubit controlled Toffoli gate $\Lambda_4(X)$ requires more gates as well as more connectivity between qubits. We test the standard one-oracle Grover's algorithm D5M5 on the sixteen-qubit processor Guadalupe (only six qubits are used by our circuits). We choose the six qubits with least two-qubit gate errors. The probability of finding the target string is degraded to a lower value than the probability of finding the non-target string. See the results listed in Table 1. The selectivity is below 1, which implies the failure of the algorithm. Classical unstructured search with one oracle can find the target string with the probability 0.0625: randomly pick up a string then verify it with the oracle; if it is not the target string then randomly pick up another one ($\frac{1}{2^5} + \frac{2^5-1}{2^5} \times \frac{1}{2^5-1} = 0.0625$). The quantum search D5M5 (with the averaged success probability of 0.0257) is worse than the classical case. Similar results on the average target states can be found in Table 13 in "Appendix B".

Although there are plenty of implementations of the five-qubit one-oracle search via the local diffusion operators, most of them give failed results (selectivity less than 1 and success probability less than classical search). However, we found that the classical-quantum hybrid search circuits G2D3M3 and G3D2M2 have selectivities larger than 1, see Table 1. G2D3M3 gives success probability higher than random pick, but relatively same as the classical search. G3D2M2 gives the average success probability 0.0963, which is higher than the classical algorithm (with one oracle). G3D2M2 randomly chooses three bits to perform the normalized two-qubit search algorithm. Since there are more two-qubit gates acting on the two qubits to be searched, we choose the physical two qubits with least errors of two-qubit gates. In our setup, physical qubits 13 and 14 are chosen, see Fig. 1. The theoretical success probability is $1/8 = 0.125$, since the two-qubit search with one oracle has 1 as the success probability. Theoretically, G3D2M2 has only half success probability compared to D5M5. In practical, the success probability of G3D2M2 is three times higher than Grover's algorithm D5M5 because of its shallow depth. In the three- and four-qubit cases, such hybrid classical-quantum circuits always have the largest selectivity (see Figs. 2 and 4). Thus, we can expect that the five-qubit search G3D2M2 stands out in the five-qubit search implementations.

Based on the success of G2D3M3 and G3D2M2, we test the divide-and-conquer circuits D2M2|D3M3 and D3M3|D2M2, which replace the random guesses in G2D3M3 and G3D2M2 by the quantum partial search algorithms. Although we have selectivities of G2D3M3 and G3D2M2 larger than 1, the selectivities D2M2|D3M3 and D3M3|D2M2 are less than 1. It suggests that the quantum partial search algorithm in the first stage is not efficient, which does not provide quantum speedup.

Table 1 Results on the five-qubit search circuits

Circuits	P_{theo}	P_{guada}	S_{guada}	d_{guada}	$\langle d_{\text{guada}} \rangle_{\text{theo}}$	$\langle d_{\text{guada}} \rangle$
D5M5†	0.258	0.0257 ± 0.0038	0.363 ± 0.076	122.37	474.30	4856.75 ± 675.33
G2D3M3	0.195	0.0654 ± 0.0087	1.880 ± 0.355	82.00	420.51	1276.61 ± 174.98
G3D2M2	0.125	0.0963 ± 0.0021	8.282 ± 1.039	53.53	428.24	556.02 ± 24.67
D2M2|D3M3	0.268	0.0667 ± 0.0150	0.904 ± 0.215	135.53	505.71	2121.44 ± 434.46
D3M3|D2M2	0.289	0.1014 ± 0.0283	0.764 ± 0.313	135.67	469.45	1444.97 ± 395.33

Circuit names with † are the standard Grover's algorithms. Standard deviations are obtained from 30×8192 shots with random target states

5 Conclusion

In this paper, we have implemented the three-, four- and five-qubit search algorithms on the IBM quantum processors. Grover's algorithm does not provide the optimal performance on the NISQ devices. To reduce the noise, we have designed the quantum search circuits using the local diffusion operators. There are three different strategies to exploit the local diffusion operators. We realized the four-qubit search algorithm with the highest success probability compared to other studies. We also successfully ran the five-qubit search algorithm on the IBM quantum devices for the first time. Additionally, the use of multi-stage circuits makes it possible to run the search in parallel. We envision our work still be useful in post-NISQ era, since the lower depth circuits would require less resources for the error corrections.

Acknowledgements This research used resources of the Oak Ridge Leadership Computing Facility, which is a DOE Office of Science User Facility supported under Contract DE-AC05-00OR22725. This material is based upon work supported by the U.S. Department of Energy, Office of Science, National Quantum Information Science Research Centers, Co-design Center for Quantum Advantage (C2QA) under contract number DE-SC0012704. P. R. participated in a program hosted by the Mathematical Sciences Research Institute in Berkeley, California, during the Spring 2021 semester, which is supported by the National Science Foundation under Grant No. DMS-1928930.

A Supplementary data for random target states

Calibration parameters of the IBM quantum processors (for the random target states) are listed in Table 2. The calibration data was retrieved at the time when the circuits were implemented. The thirty random chosen target states for the three-, four-, and five-qubit search are listed in Table 3. The explanations on the three-qubit circuits are listed in Tables 4, 5. The experimental results for the three-qubit circuits are presented in Table 6. The naming convention for the four-qubit circuits are listed in Table 7. The theoretical and experimental data for the four-qubit search circuits are presented in Tables 8 and 9, respectively.

Table 2 Calibration specs for the IBM quantum processors were retrieved on the day of data (for random target states)

Backends	CNOT error	Readout error	T_1	T_2	Quantum volume	Version	Date
Vigo	8.627e−3	3.222e−2	98.13	66.88	16	1.3.5	Jan. 9, 2021
Athens	9.262e−3	1.842e−2	84.55	102.56	32	1.3.6	Jan. 17, 2021
Guadalupe	1.245e−2	2.056e−2	78.15	90.72	32	1.2.18	June 12, 2021

Table 3 Thirty random generated target states for the three-, four-, and five-qubit search algorithms

Number of qubits	Thirty random target states									
	001	101	010	001	001	111	010	111	001	100
Three	011	000	100	111	010	011	110	111	110	011
	101	111	110	001	001	000	001	001	001	001
	1001	1101	1010	0001	1110	0010	1001	0100	0011	0111
Four	0001	0101	1110	0000	1010	1010	0101	0011	0001	0000
	1100	0110	1111	0111	0000	0101	1101	1111	1000	0111
	01010	10001	01011	01000	11111	00000	00000	00100	01010	00010
Five	01011	11100	10101	11010	00100	10100	01010	11001	01100	10001
	00011	01101	00011	10000	10100	10000	11000	10100	11111	11000

Table 4 Naming explanations for the three-qubit search circuits

Circuits	Oracle numbers	Initial state	Operation	Measurement	Remarks on the second stage
D3M3†	1	$H^{\otimes 3}\|0\rangle^{\otimes 3}$	G_3	All qubits	NA
D2M3	1	$H^{\otimes 3}\|0\rangle^{\otimes 3}$	G_2	All qubits	NA
G1D2M2	1	$\|t_1\rangle \otimes H^{\otimes 2}\|0\rangle^{\otimes 2}$	G_2	Qubits of $\|t_2t_3\rangle$	NA
D3D3M3†	2	$H^{\otimes 3}\|0\rangle^{\otimes 3}$	G_3^2	All qubits	NA
D3M1|D2M2	2	$H^{\otimes 3}\|0\rangle^{\otimes 3}$	G_3	Qubit of $\|t_1\rangle$	Equivalent to G1D2M2
D2M1|D2M2	2	$H^{\otimes 3}\|0\rangle^{\otimes 3}$	G_2	Qubit of $\|t_1\rangle$	Equivalent to G1D2M2

Suppose that the target string is $t_1t_2t_3$, corresponding to the target state $|t_1t_2t_3\rangle$. Circuit names with † are the standard Grover's algorithms

Table 5 Parameters of the three-qubit search circuits on the Vigo and Athens

Circuits	P_{theo}	$d_{\text{vigo}}^{(1)}, d_{\text{vigo}}^{(2)}$	$\langle d_{\text{vigo}}\rangle_{\text{theo}}$	$d_{\text{athens}}^{(1)}, d_{\text{athens}}^{(2)}$	$\langle d_{\text{athens}}\rangle_{\text{theo}}$
D3M3†	0.781	39.43	50.47	40.03	51.24
D2M3	0.5	32.30	64.60	33.17	66.33
G1D2M2	0.5	28.70	57.40	29.73	59.47
D3D3M3†	0.945	67.83	71.76	68.63	72.60
D3M1|D2M2	0.875	39.43, 28.70	79.73	40.03, 29.73	79.73
D2M1|D2M2	0.750	31.87, 28.70	83.87	33.17, 29.73	83.87

Circuit names with † are the standard Grover's algorithms

B Supplementary data for average target states

Calibration parameters of the IBM quantum processors (for the average target states) are listed in Table 10. The results for the three-, four-, and five-qubit search based on the average target states are listed in Tables 11, 12 and 13, respectively.

Table 6 Success probabilities, selectivities and depths of the three-qubit search circuits

Circuits	P_{vigo}	S_{vigo}	$\langle d_{\text{vigo}} \rangle$	P_{athens}	S_{athens}	$\langle d_{\text{athens}} \rangle$
D3M3†	0.538 ± 0.042	5.86 ± 1.59	73.58 ± 3.29	0.559 ± 0.022	5.36 ± 0.99	71.71 ± 3.29
D2M3	0.407 ± 0.033	2.70 ± 0.40	79.52 ± 3.09	0.400 ± 0.013	2.88 ± 0.15	83.00 ± 5.28
G1D2M2	0.415 ± 0.019	14.65 ± 3.70	66.49 ± 3.20	0.443 ± 0.019	19.66 ± 4.49	66.60 ± 3.18
D3D3M3†	0.575 ± 0.044	7.10 ± 1.93	118.29 ± 8.16	0.638 ± 0.027	8.44 ± 1.73	107.67 ± 4.13
D3M1|D2M2	0.635 ± 0.042	3.28 ± 0.40	107.58 ± 6.58	0.657 ± 0.025	2.89 ± 0.30	106.31 ± 7.11
D2M1|D2M2	0.604 ± 0.038	2.67 ± 0.25	100.61 ± 6.44	0.621 ± 0.017	2.35 ± 0.13	101.26 ± 5.87

Circuit names with † are the standard Grover's algorithms. Standard deviations are obtained from 30 trials with random target states. Each trial has 8192 shots

Table 7 Naming explanations for the four-qubit search circuits

Circuits	Oracle numbers	Initial state	Operation	Measurement	Remarks on the second stage
D4M4†	1	$H^{\otimes 4}\|0\rangle^{\otimes 4}$	G_4	All qubits	NA
D3M4	1	$H^{\otimes 4}\|0\rangle^{\otimes 4}$	G_3	All qubits	NA
D2M4	1	$H^{\otimes 4}\|0\rangle^{\otimes 4}$	G_2	All qubits	NA
G1D3M3	1	$\|t_1\rangle \otimes H^{\otimes 3}\|0\rangle^{\otimes 3}$	G_3	Qubits of $\|t_2 t_3 t_4\rangle$	NA
G2D2M2	1	$\|t_1 t_2\rangle \otimes H^{\otimes 2}\|0\rangle^{\otimes 2}$	G_2	Qubits of $\|t_3 t_4\rangle$	NA
D4D4M4†	2	$H^{\otimes 4}\|0\rangle^{\otimes 4}$	G_4^2	All qubits	NA
D3D4M4	2	$H^{\otimes 4}\|0\rangle^{\otimes 4}$	$G_4 G_3$	All qubits	NA
D2D4M4	2	$H^{\otimes 4}\|0\rangle^{\otimes 4}$	$G_4 G_2$	All qubits	NA
D4M1|D3M32		$H^{\otimes 4}\|0\rangle^{\otimes 4}$	G_4	Qubit of $\|t_1\rangle$	Equivalent to G1D3M3
D3M1|D3M32		$H^{\otimes 4}\|0\rangle^{\otimes 4}$	G_3	Qubit of $\|t_1\rangle$	Equivalent to G1D3M3
D2M1|D3M32		$H^{\otimes 4}\|0\rangle^{\otimes 4}$	G_2	Qubit of $\|t_1\rangle$	Equivalent to G1D3M3
D4M2|D2M22		$H^{\otimes 4}\|0\rangle^{\otimes 4}$	G_4	Qubits of $\|t_1 t_2\rangle$	Equivalent to G2D2M2
D3M2|D2M22		$H^{\otimes 4}\|0\rangle^{\otimes 4}$	G_3	Qubits of $\|t_1 t_2\rangle$	Equivalent to G2D2M2
D2M2|D2M22		$H^{\otimes 4}\|0\rangle^{\otimes 4}$	G_2	Qubits of $\|t_1 t_2\rangle$	Equivalent to G2D2M2

Suppose that the target string is $t_1 t_2 t_3 t_4$, corresponding to the target state $|t_1 t_2 t_3 t_4\rangle$. Circuit names with † are the standard Grover's algorithms

Table 8 Parameters of the four-qubit search circuits on the Vigo and Athens

Circuits	P_{theo}	$d^{(1)}_{\text{vigo}}, d^{(2)}_{\text{vigo}}$	$\langle d_{\text{vigo}}\rangle_{\text{theo}}$	$d^{(1)}_{\text{athens}}, d^{(2)}_{\text{athens}}$	$\langle d_{\text{athens}}\rangle_{\text{theo}}$
D4M4†	0.473	86.07	182.07	130.87	276.85
D3M4	0.390	74.00	189.65	83.70	214.51
D2M4	0.250	34.97	139.87	47.87	191.47
G1D3M3	0.391	74.00	189.43	83.70	214.26
G2D2M2	0.250	34.97	139.87	46.73	186.93
D4D4M4†	0.908	161.13	177.38	250.27	275.50
D3D4M4	0.821	166.13	202.28	207.00	252.04
D2D4M4	0.660	99.57	150.81	140.87	213.37
D4M1|D3M3	0.561	72.07, 74.00	260.35	104.80, 83.70	336.10
D3M1|D3M3	0.537	74.00, 74.00	275.53	83.70, 83.70	311.65
D2M1|D3M3	0.488	34.77, 74.00	222.75	47.80, 83.70	269.30
D4M2|D2M2	0.578	72.33, 34.97	185.61	105.20, 46.73	262.81
D3M2|D2M2	0.531	74.00, 34.97	205.09	83.70, 46.73	245.50
D2M2|D2M2	0.438	34.97, 34.97	159.85	47.93, 46.73	216.38

Circuit names with † are the standard Grover's algorithms

Table 9 Success probabilities, selectivities and depths of the four-qubit search circuits on IBM's Vigo and Athens machines

Circuits	P_{vigo}	S_{vigo}	$\langle d_{\text{vigo}}\rangle$	P_{athens}	S_{athens}	$\langle d_{\text{athens}}\rangle$
D4M4†	0.165 ± 0.018	1.91 ± 0.17	526.66 ± 54.17	0.181 ± 0.010	2.28 ± 0.33	725.65 ± 41.46
D3M4	0.195 ± 0.019	2.10 ± 0.37	382.49 ± 39.23	0.208 ± 0.016	1.90 ± 0.28	404.27 ± 31.08
D2M4	0.173 ± 0.013	2.06 ± 0.24	203.71 ± 17.62	0.170 ± 0.008	1.78 ± 0.17	282.61 ± 15.28
G1D3M3	0.209 ± 0.018	3.69 ± 0.51	356.10 ± 44.06	0.230 ± 0.010	4.67 ± 0.41	364.03 ± 11.11
G2D2M2	0.199 ± 0.019	8.43 ± 1.99	176.24 ± 10.40	0.211 ± 0.004	13.36 ± 2.76	221.21 ± 5.72
D4D4M4†	0.195 ± 0.022	2.19 ± 0.17	833.99 ± 83.83	0.183 ± 0.018	2.03 ± 0.38	1378.31 ± 136.04
D3D4M4	0.151 ± 0.017	1.76 ± 0.16	1110.15 ± 116.23	0.205 ± 0.013	2.44 ± 0.40	1013.44 ± 64.76
D2D4M4	0.197 ± 0.023	2.15 ± 0.20	513.59 ± 60.89	0.195 ± 0.019	2.41 ± 0.31	727.35 ± 64.34
D4M1|D3M3	0.264 ± 0.055	1.46 ± 0.16	570.74 ± 88.11	0.282 ± 0.012	1.58 ± 0.06	670.76 ± 28.76
D3M1|D3M3	0.253 ± 0.038	1.46 ± 0.18	595.99 ± 83.11	0.286 ± 0.017	1.64 ± 0.11	586.68 ± 28.91
D2M1|D3M3	0.249 ± 0.038	1.40 ± 0.13	443.90 ± 50.68	0.286 ± 0.014	1.64 ± 0.10	460.51 ± 18.70
D4M2|D2M2	0.311 ± 0.045	1.58 ± 0.17	351.38 ± 42.16	0.324 ± 0.015	1.87 ± 0.17	444.56 ± 20.50
D3M2|D2M2	0.314 ± 0.042	1.68 ± 0.23	352.18 ± 37.03	0.333 ± 0.021	1.78 ± 0.19	392.85 ± 21.87
D2M2|D2M2	0.345 ± 0.077	1.70 ± 0.19	211.35 ± 39.81	0.335 ± 0.043	1.70 ± 0.37	287.58 ± 39.97

Circuit names with † are the standard Grover's algorithms. Standard deviations are obtained from 30 trials with random target states. Each trial has 8192 shots

Table 10 Calibration specs for the IBM quantum processors were retrieved on the day of data (for average target states)

Backends	CNOT error	Readout error	T_1	T_2	Quantum volume	Version	Date
Athens	1.212e−2	1.476e−2	85.96	78.79	32	1.3.19	June 9, 2021
Guadalupe	1.245e−2	2.056e−2	78.15	90.72	32	1.2.18	June 12, 2021

Table 11 Success probabilities, selectivities and depths of the three-qubit search with average target states

Circuits	P_{athens} (P_{highest}, P_{lowest})	S_{athens}	$\langle d_{\text{athens}} \rangle$
D3M3†	0.526 ± 0.028 (0.550, 0.470)	5.38 ± 0.78	76.26 ± 3.57
D2M3	0.370 ± 0.018 (0.380, 0.335)	2.48 ± 0.13	94.93 ± 6.56
G1D2M2	0.441 ± 0.018 (0.453, 0.425)	18.02 ± 5.60	22.09 ± 2.14
D3D3M3†	0.616 ± 0.025 (0.660, 0.593)	8.15 ± 0.90	110.92 ± 2.57
D3M1|D2M2	0.645 ± 0.030 (0.691, 0.582)	2.77 ± 0.29	92.03 ± 3.18
D2M1|D2M2	0.611 ± 0.016 (0.638, 0.594)	2.26 ± 0.14	87.73 ± 4.05

Circuit names with † are the standard Grover's algorithms. Standard deviations are obtained from eight trails (with eight different target states). Each trial has 8192 shots

Table 12 Success probabilities, selectivities and depths of the four-qubit search with average target states

Circuits	P_{athens} (P_{highest}, P_{lowest})	S_{athens}	$\langle d_{\text{athens}} \rangle$
D4M4†	0.177 ± 0.016 (0.207, 0.157)	2.15 ± 0.46	744.81 ± 59.87
D3M4	0.209 ± 0.014 (0.231, 0.175)	2.01 ± 0.15	401.15 ± 25.07
D2M4	0.178 ± 0.010 (0.193, 0.152)	1.98 ± 0.15	269.56 ± 18.53
G1D3M3	0.218 ± 0.014 (0.237, 0.185)	4.03 ± 0.37	384.65 ± 22.82
G2D2M2	0.211 ± 0.06 (0.219, 0.200)	13.60 ± 3.62	221.79 ± 59.09
D4D4M4†	0.163 ± 0.014 (0.196, 0.137)	1.87 ± 0.28	1548.59 ± 129.69
D3D4M4	0.219 ± 0.015 (0.253, 0.200)	2.71 ± 0.35	947.37 ± 60.44
D2D4M4	0.188 ± 0.017 (0.217, 0.161)	2.23 ± 0.22	757.44 ± 65.97
D4M1|D3M3	0.263 ± 0.017 (0.298, 0.231)	1.53 ± 0.12	720.55 ± 45.95
D3M1|D3M3	0.268 ± 0.024 (0.305, 0.213)	1.60 ± 0.16	628.39 ± 56.31
D2M1|D3M3	0.269 ± 0.022 (0.306, 0.222)	1.62 ± 0.16	490.25 ± 36.06
D4M2|D2M2	0.328 ± 0.016 (0.346, 0.294)	1.73 ± 0.13	463.54 ± 25.87
D3M2|D2M2	0.339 ± 0.015 (0.360, 0.305)	1.86 ± 0.16	385.39 ± 15.82
D2M2|D2M2	0.364 ± 0.015 (0.382, 0.336)	2.14 ± 0.16	259.73 ± 11.33

Circuit names with † are the standard Grover's algorithms. Standard deviations are obtained from sixteen trails (with sixteen different target states). Each trial has 8192 shots

Table 13 Success probabilities, selectivities and depths of the five-qubit search with average target states

Circuits	P_{guada} (P_{highest}, P_{lowest})	S_{guada}	$\langle d_{\text{guada}} \rangle$
D5M5†	0.0392 ± 0.0606 (0.0522, 0.0184)	0.656 ± 0.154	3072.73 ± 857.30
G2D3M3	0.0570 ± 0.0050 (0.0636, 0.0471)	1.453 ± 0.164	1263.78 ± 111.71
G3D2M2	0.0985 ± 0.0025 (0.1038, 0.0942)	8.971 ± 1.355	444.13 ± 8.45
D2M2|D3M3	0.0576 ± 0.0109 (0.0779, 0.0371)	0.884 ± 0.192	2078.96 ± 429.64
D3M3|D2M2	0.1135 ± 0.0284 (0.1568, 0.0647)	0.804 ± 0.310	1093.12 ± 322.35

Circuit names with † are the standard Grover's algorithms. Standard deviations are obtained from thirty two trails (with thirty two different target states). Each trial has 8192 shots

References

1. Barends, R., Kelly, J., Megrant, A., Veitia, A., Sank, D., Jeffrey, E., White, T.C., Mutus, J., Fowler, A.G., Campbell, B., et al.: Superconducting quantum circuits at the surface code threshold for fault tolerance. Nature **508**(7497), 500 (2014)
2. Ballance, C.J., Harty, T.P., Linke, N.M., Sepiol, M.A., Lucas, D.M.: High-fidelity quantum logic gates using trapped-ion hyperfine qubits. Phys. Rev. Lett. **117**(6), 060504 (2016)
3. Figgatt, C., Maslov, D., Landsman, K.A., Linke, N.M., Debnath, S., Monroe, C.: Complete 3-qubit grover search on a programmable quantum computer. Nat. Commun. **8**(1), 1918 (2017)
4. Google AI Quantum, et al.: Hartree-fock on a superconducting qubit quantum computer. Science **369**(6507), 1084–1089 (2020)
5. Arute, F., Arya, K., Babbush, R., Bacon, D., Bardin, J.C., Barends, R., Biswas, R., Sergio, B., Fernando, G.S.L., Buell, D.A., et al.: Quantum supremacy using a programmable superconducting processor. Nature **574**(7779), 505–510 (2019)
6. Zhong, H.-S., Wang, H., Deng, Y.-H., Chen, M.-C., Peng, L.-C., Luo, Y.-H., Qin, J., Wu, D., Ding, X., Hu, Y., et al.: Quantum computational advantage using photons. Science **370**(6523), 1460–1463 (2020)
7. Nielsen, M.A., Chuang, I.L.: Quantum computation and quantum information, (2010)
8. Preskill, J.: Quantum computing in the nisq era and beyond. Quantum **2**, 79 (2018)
9. Cross, A.W., Bishop, L.S., Sheldon, S., Nation, P.D., Gambetta, J.M.: Validating quantum computers using randomized model circuits. Phys. Rev. A **100**(3), 032328 (2019)
10. Bharti, K., Cervera-Lierta, A., Kyaw, T.H., Haug, T., Alperin-Lea, S., Anand, A., Degroote, M., Heimonen, H., Kottmann, J.S., Menke, T., Mok, W.-K., Sim, S., Kwek, L.-C., Aspuru-Guzik, A.: Noisy intermediate-scale quantum (nisq) algorithms. arXiv preprint arXiv:2101.08448, (2021)
11. Grover, L.K.: Quantum mechanics helps in searching for a needle in a haystack. Phys. Rev. Lett. **79**(2), 325 (1997)
12. Giri, P.R., Korepin, V.E.: A review on quantum search algorithms. Quantum Inf. Process. **16**(12), 315 (2017)
13. Bennett, C.H., Bernstein, E., Brassard, G., Vazirani, U.: Strengths and weaknesses of quantum computing. SIAM J. Comput. **26**(5), 1510–1523 (1997)
14. Biamonte, J., Wittek, P., Pancotti, N., Rebentrost, P., Wiebe, N., Lloyd, S.: Quantum machine learning. Nature **549**(7671), 195–202 (2017)
15. Boyer, M., Brassard, G., Høyer, P., Tapp, A.: Tight bounds on quantum searching. Fortschritte der Physik: Prog. Phys. **46**(4–5), 493–505 (1998)
16. Zalka, C.: Grover's quantum searching algorithm is optimal. Phys. Rev. A **60**(4), 2746 (1999)
17. Grassl, M., Langenberg, B., Roetteler, M., Steinwandt, R.: Applying grover's algorithm to aes: quantum resource estimates. In: Post-Quantum Cryptography, pp. 29–43. Springer, (2016)
18. Kim, P., Han, D., Jeong, K.C.: Time-space complexity of quantum search algorithms in symmetric cryptanalysis: applying to aes and sha-2. Quantum Inf. Process. **17**(12), 339 (2018)
19. Jaques, S., Naehrig, M., Roetteler, M., Virdia, F.: Implementing grover oracles for quantum key search on aes and lowmc. In: Annual International Conference on the Theory and Applications of Cryptographic Techniques, pp. 280–310. Springer, (2020)

20. Wang, Y., Krstic, P.S.: Prospect of using grover's search in the noisy-intermediate-scale quantum-computer era. Phys. Rev. A **102**(4), 042609 (2020)
21. Kato, G.: Grover-algorithm-like operator using only single-qubit gates. Phys. Rev. A **72**(3), 032319 (2005)
22. Tulsi, A.: Faster quantum searching with almost any diffusion operator. Phys. Rev. A **91**(5), 052307 (2015)
23. Jiang, Z., Rieffel, E.G., Wang, Z.: Near-optimal quantum circuit for grover's unstructured search using a transverse field. Phys. Rev. A **95**(6), 062317 (2017)
24. Grover, L.K., Radhakrishnan, J.: Is partial quantum search of a database any easier? In: Proceedings of the seventeenth annual ACM symposium on Parallelism in algorithms and architectures, pp. 186–194. ACM, (2005)
25. Korepin, V.E.: Optimization of partial search. J. Phys. A Math. General **38**(44), L731 (2005)
26. Korepin, V.E., Grover, L.K.: Simple algorithm for partial quantum search. Quantum Inf. Process. **5**, 5–10 (2006)
27. Grover, L.K.: Trade-offs in the quantum search algorithm. Phys. Rev. A **66**(5), 052314 (2002)
28. Briański, M., Gwinner, J., Hlembotskyi, V., Jarnicki, W., Pliś, S., Szady, A.: Introducing structure to expedite quantum search. arXiv preprint arXiv:2006.05828, (2020)
29. Zhang, K., Korepin, V.E.: Depth optimization of quantum search algorithms beyond grover's algorithm. Phys. Rev. A **101**(3), 032346 (2020)
30. Liu, J., Zhou, H.: Hardware efficient quantum search algorithm. arXiv preprint arXiv:2103.14196, (2021)
31. Mandviwalla, A., Ohshiro, K., Ji, B.: Implementing grover's algorithm on the ibm quantum computers. In: 2018 IEEE International Conference on Big Data (Big Data), pp. 2531–2537. IEEE, (2018)
32. Gwinner, J., Briański, M., Burkot, W., Czerwiński, Ł., Hlembotskyi, V.: Benchmarking 16-element quantum search algorithms on ibm quantum processors. arXiv preprint arXiv:2007.06539, (2020)
33. Satoh, T., Ohkura, Y., Van Meter, R.: Subdivided phase oracle for nisq search algorithms. arXiv preprint arXiv:2001.06575, (2020)
34. Hlembotskyi, V., Burczyński, R., Jarnicki, W., Szady, A., Tułowiecki, J.: Efficient unstructured search implementation on current ion-trap quantum processors. arXiv preprint arXiv:2010.03841, (2020)
35. Grover, L.K.: Quantum computers can search rapidly by using almost any transformation. Phys. Rev. Lett. **80**(19), 4329 (1998)
36. Brassard, G., Hoyer, P., Mosca, M., Tapp, A.: Quantum amplitude amplification and estimation. Contemp. Math. **305**, 53–74 (2002)
37. Almazrooie, M., Samsudin, A., Abdullah, R., Mutter, K.N.: Quantum reversible circuit of aes-128. Quantum Inf. Process. **17**(5), 112 (2018)
38. Langenberg, B., Pham, H., Steinwandt, R.: Reducing the cost of implementing aes as a quantum circuit. Technical report, Cryptology ePrint Archive, Report 2019/854, (2019)
39. Barenco, A., Bennett, C.H., Cleve, R., DiVincenzo, D.P., Margolus, N., Shor, P., Sleator, T., Smolin, J.A., Weinfurter, H.: Elementary gates for quantum computation. Phys. Rev. A **52**(5), 3457 (1995)
40. Korepin, V.E., Liao, J.: Quest for fast partial search algorithm. Quantum Inf. Process. **5**(3), 209–226 (2006)
41. Korepin, V.E., Vallilo, B.C.: Group theoretical formulation of a quantum partial search algorithm. Prog. Theor. Phys. **116**(5), 783–793 (2006)
42. Gingrich, R.M., Williams, C.P., Cerf, N.J.: Generalized quantum search with parallelism. Phys. Rev. A **61**(5), 052313 (2000)
43. Maslov, D.: Advantages of using relative-phase toffoli gates with an application to multiple control toffoli optimization. Phys. Rev. A **93**(2), 022311 (2016)
44. Song, G., Klappenecker, A.: Optimal realizations of simplified toffoli gates. Quantum Inf. Comput. **4**(5), 361–372 (2004)
45. Tannu, S.S., Qureshi, M.: Ensemble of diverse mappings: Improving reliability of quantum computers by orchestrating dissimilar mistakes. In: Proceedings of the 52nd Annual IEEE/ACM International Symposium on Microarchitecture, pp. 253–265 (2019)